

A Hydro-elastic Model of Hydrocephalus

A. Smillie¹, I. Sobey² & Z. Molnar³

We combine elements of poroelasticity and of fluid mechanics to construct a mathematical model of the human brain and ventricular system. The model is used to study hydrocephalus, a pathological condition in which the normal flow of the cerebrospinal fluid is disturbed, causing the brain to become deformed. Our model extends recent work in this area by including flow through the aqueduct, by incorporating boundary conditions which we believe more accurately represent the anatomy of the brain and by including time dependence. This enables us to construct a quantitative model of the onset, development and treatment of this condition. We formulate and solve the governing equations and boundary conditions for this model and give results which are relevant to clinical observations.

¹Present address: Imperial College, London

² Corresponding author ³Department of Human Anatomy, Oxford

1 Introduction

Hydrocephalus is an illness in which abnormal flow of cerebrospinal fluid (CSF) through the cerebral ventricular system causes the brain to become deformed. The disease itself is well known, due both to its relatively high incidence and to its debilitating and often fatal effects (Drake and Sainte-Rose, 1995). Despite the level of awareness and the progress which has been made in recent decades in understanding the condition, a treatment which is both reliable and widely applicable remains elusive, see Drake et al. (1998).

CSF is produced mainly in the choroid plexuses; long, convoluted strands of vascularized tissue located in the the lateral, third and fourth ventricles. The mechanism by which fluid is produced and secreted is rather complex, but the production rate of around 500 ml/day in human adults is well known and is reported to be independent of external influences such as intraventricular pressure (Bradbury, 1993). Given that the total volume of the cerebral ventricular system is around 150 ml we may suppose that the CSF is renewed about three times daily.

In a healthy brain, CSF flows from production sites in the choroid plexuses of the lateral and third ventricles through a single narrow cerebral aqueduct and into a fourth ventricle. It then moves through another series of narrow passageways known as the median and lateral apertures into the pontine cistern and cisterna magna near the base of the skull, from where it passes into the subarachnoid space between the brain and the dura matter. A little fluid is also believed to flow down the subarachnoid space around the spinal cord and then flow back up into the cranial subarachnoid space, though it seems difficult to explain how this flow could be maintained in terms of fluid mechanics.

CSF absorption occurs in the arachnoid villi, small granulations of the arachnoid which protrude into the dura matter. The barrier between the CSF and the blood in these granulations is thin, enabling CSF to pass into the bloodstream where it is absorbed. In contrast with CSF production, the rate of absorption is pressure dependent, specifically depending upon the difference between the intraventricular pressure and the superior sagittal venous pressure (Bradbury, 1993). The structure of the arachnoid villi is such that even in the unlikely event of venous blood pressure exceeding the intraventricular pressure no flow will take place from the blood into the CSF system, so that the villi effectively act as a one-way valve for removal of CSF.

The build up of fluid associated with hydrocephalus may in theory be caused by overproduction of CSF in the ventricles, under-absorption in the subarachnoid space or some obstruction of the CSF pathways. With the exception of a few rare cases it is the latter of these which is the cause of the illness.

Obstruction of the CSF pathways can happen at any point in the ventricular system, but the long, narrow aqueduct of Sylvius which runs between the third and fourth ventricles is reported as being the most frequent site for a blockage to occur (Weller et al., 1993). There is in the literature the descriptors, connecting and non-connecting hydrocephalus to distinguish cases where the aqueduct is open or blocked but since we are interested in the whole range of states of the aqueduct we shall not use these here. The potential causes of a blockage in the flow pathways are many and varied. The most frequent cause of congenital and infantile hydrocephalus is a malformation in one or more parts of the ventricular system, for example stenosis of the aqueduct or membranous occlusion of the foramen of Monro. A blockage can also be the result of a blood clot entering the CSF system and occluding the aqueduct. Hydrocephalus has also been known to occur as a result of occluded flow pathways in the

subarachnoid space itself, though this is relatively rare.

A consequence of the disease is normally oedema of the parenchyma, particularly the white matter adjacent to the ventricles. It is this oedema, together with the deformation of the brain itself that is the cause of most of the long term tissue damage associated with hydrocephalus, which can result in a range of symptoms including headaches, gait disorder, intellectual impairment and ultimately death.

A traditional approach to modelling hydrocephalus is a lumped parameter model where the contents of the skull are represented by a series of interconnected compartments through which fluid is exchanged. All of the resistance to flow between these compartments is lumped at these interfaces. The formulation of such models leads to a system of coupled differential equations for the evolution in time of the fluid pressure in each compartment. The solution of that system gives a relationship between the intracranial pressure and the volume of the ventricles, see for instance Sivaloganathan et al. (1998). Such a pressure-volume relationship is useful to clinicians in the diagnosis and treatment of hydrocephalus but the chief weakness of the approach is that no spatial variation is permitted in any of the physical parameters, hence it is not possible to describe the stress and strain distributions in the brain tissue or to make predictions regarding the distribution of fluid in hydrocephalus. Such significant limitations mean that over the last decade attention has shifted away from lumped parameter models to the formulation of a spatially more realistic models for the hydrocephalic brain.

A number of authors have proposed mechanical models of hydrocephalus based on the theory of poroelasticity. It is hoped that such models will give a better understanding of the condition and hence better treatment. These existing poroelastic models consider hydrocephalus in the final diseased state and do not consider the transition from the healthy to the pathological condition of the brain when there is still be flow through the aqueduct. Nor have such models included the transient effects associated with shunting, the most widely used treatment for hydrocephalus. In this paper we construct a model of the brain and ventricular system which is sufficiently complex to reproduce the behaviour of the hydrocephalic brain yet simple enough to be mathematically tractable, and use the model to analyse the onset and treatment of the condition. A review of the general area of application of poroelasticity to the brain may be found in Tenti et al. (2000).

The use of a mechanical model with a more realistic spherical geometry was first proposed in Hakim et al. (1976), as was the concept of the brain as a spongelike material. The governing equations formulated by Hakim *et al* do not however incorporate this spongelike behaviour and so are unable to simulate the build up of fluid in brain tissue (oedema) observed in cases of hydrocephalus.

A crucial step forward was made by Nagashima et al. (1987), who used the consolidation theory developed by Biot (1941) to model the brain as a porous, linearly elastic solid. This enabled them to formulate governing equations which modelled both the stress and strain distribution and the pressure of distribution of fluid (CSF) through the brain. These authors used a finite element method to solve their model numerically for an anatomically realistic geometry. While this approach yielded results which were in qualitative agreement with clinical observations, the quantitative accuracy of their results was limited by their use of inaccurate values of some the material parameters and by the somewhat naive boundary conditions used in solving the governing equations.

Recent papers by Kaczmarek et al. (1997), Tenti et al. (1998) and Levine (1999) have attempted to resolve these difficulties with varying degrees of success. In Kaczmarek et al.

(1997) and Tenti et al. (1998) a cylindrical geometry is used in order to facilitate the analytic solution of the governing equations. Such analytic solutions are desirable as they give a deeper insight into the behaviour of pressure and stress through the brain, but the use of such a geometry seems somewhat unreasonable, especially when it comes to specifying boundary conditions at the ends of the cylindrical ‘brain’. Levine uses a spherically symmetric geometry similar to that in Hakim et al. (1976) to construct analytic solutions and Stastna et al. (1998) extended the model in Tenti et al. (1998) to include some transient effects.

All of the authors model the brain as a poroelastic solid undergoing small strains, Kaczmarek *et al* and Tenti *et al* use data from a range of medical and anatomical studies to find the values of for example, the Young’s modulus and permeability of the brain tissue. Levine modified previous poroelastic models by attempting to incorporate the absorption of fluid in the brain tissue and the effect of the venous bed in the skull. This approach necessitated the use of more physical parameters and the results of Levine and Tenti *et al* are qualitative in nature. The model of Kaczmarek et al. (1997) was able provide predictions for flow and stress in the brain tissue.

In the next section we set out the results from poroelasticity and fluid flow which we use in our model. Then we describe the assumptions regarding geometry, material properties and time dependence which we make in order to complete a model of hydrocephalus. We then present solutions to the model and consider the physical parameters which we shall require in order to make quantitative predictions about the behaviour of the brain and CSF. These solutions are discussed in terms of their usefulness relative to some of the other models available and their consistency with clinical data.

2 Mathematical Model

In this section we set out some basic results from poroelasticity and fluid mechanics which underly our model of the brain. As already indicated, the model can be applied to a healthy or a damaged cerebrospinal fluid flow. We will assume that CSF is produced at a constant rate and once produced can (a) remain in the ventricle, causing the ventricle to enlarge, (b) flow through the aqueduct or (c) flow through the porous matrix of brain tissue.

2.1 Poroelastic equations

An isotropic elastic solid subject to a stress field σ_{ij} such that it undergoes a small strain deformation with displacements u_i in the coordinate directions with a resultant strain tensor ϵ_{ij} satisfies the constitutive relationship from Hooke’s Law,

$$\epsilon_{ij} = \frac{1}{E} \left[(1 + \nu) \sigma_{ij} - \nu \sigma_{kk} \delta_{ij} \right], \quad (2.1)$$

where δ_{ij} is the Kronecker delta. The elastic constants E and ν represent the Young’s modulus and Poisson’s ratio of the material respectively. The volumetric strain, or dilation, is defined by

$$\varepsilon = \epsilon_{kk} = \frac{\partial u_k}{\partial x_k}. \quad (2.2)$$

The poroelasticity model introduced by Biot (1941) generalized the above equations to model a solid-fluid mixture by introducing a new variable, the fluid pressure, p . Equation (2.1)

became

$$\epsilon_{ij} = \frac{1}{E} \left[(1 + \nu) \sigma_{ij} - \nu \sigma_{kk} \delta_{ij} \right] + \frac{p}{3H} \delta_{ij} \quad (2.3)$$

where H was a new physical parameter which was regarded as a measure of the mixture's compressibility for a change in fluid pressure.

In order to completely describe the condition of the body we require an additional parameter ζ , the increment of fluid content. A positive value for ζ indicates that fluid has been added by the application of the stress field, a negative value indicates that fluid has been removed. By considering the isotropy of the body and assuming the existence of a potential energy of the mixture it can be shown (see, for example, Wang (2002)) that ζ is given by

$$\zeta = \frac{1}{H} \sigma_{kk} + \frac{p}{G}. \quad (2.4)$$

G is another new physical constant which describes the change in fluid content for a given change in fluid pressure.

We now invert equation (2.3) to give

$$\sigma_{ij} = \frac{E}{1 + \nu} \epsilon_{ij} + \frac{\nu E}{(1 + \nu)(1 - 2\nu)} \epsilon \delta_{ij} - \alpha p \delta_{ij}, \quad (2.5)$$

where the Biot-Willis parameter α is another poroelastic constant defined as

$$\alpha = \frac{1}{3} \frac{E}{(1 - 2\nu)H}.$$

The expression for the increment of fluid content (2.4) can be rewritten in terms of the strain

$$\zeta = \alpha \epsilon + \frac{(1 - \alpha\beta)\alpha}{K\beta} p. \quad (2.6)$$

In this expression K is the bulk modulus of the body,

$$K = \frac{E}{3(1 - 2\nu)},$$

and we denote Skempton's coefficient as β ,

$$\beta = \frac{G}{H},$$

where β is essentially a measure of how the applied stress is distributed between the solid matrix and the fluid. It tends to one for saturated mixtures where the load is supported entirely by the fluid and zero for gas filled pores where the stress is transferred through the solid. By setting $p = 0$ in (2.6) we can see that α may be interpreted as the ratio of volume of fluid displaced to the volumetric strain under drained conditions.

Note that in poroelasticity theory there exist a range of different material constants (such as G , H , α and β) which characterize the behaviour of the fluid-solid mixture, see Wang (2002) for an exhaustive list. There are however only two distinct constants which, together with two elastic constants representing the average elastic properties of the solid matrix, fully describe the material properties of the body. This is analogous to the case of isotropic linear elasticity where only two constants are ever required to completely specify the elastic properties of a

material but several elastic moduli are defined and used in practice. For consistency and simplicity we shall use E , ν , α and β as the four independent material constants. We do, however, observe that two more constants, the undrained Poisson's ratio ν_u and the undrained Young's modulus E_u , can be defined as

$$\nu_u = \frac{3\nu + \alpha\beta(1 - 2\nu)}{3 - \alpha\beta(1 - 2\nu)} \quad \text{and} \quad E_u = \frac{(1 - 2\nu_u)}{(1 - 2\nu)} \frac{E}{1 - \alpha\beta}. \quad (2.7)$$

Our reason for making these additional definitions will become evident when we consider the values of the material parameters to be used in our model.

We also observe that the total stress tensor of the mixture, σ_{ij} , may be regarded as an additive mixture of the fluid pressure p and the 'effective stress' in the solid matrix σ'_{ij} ,

$$\sigma_{ij} = \sigma'_{ij} - \alpha p \delta_{ij} \quad (2.8)$$

The negative sign on the pressure follows from the convention in solid mechanics that pressures are positive and compressive stresses negative. This idea of the separation of the total stress into solid and fluid components will be useful in the application of the boundary conditions.

2.2 Fluid flow equations

In order to completely model the behaviour of a fluid-solid mixture we also require an expression for the movement of fluid through the solid matrix. We use D'Arcy's Law for the flow of fluid through a porous medium, which for spherically symmetric flow with radius r , is

$$W = -\frac{k}{\mu} \frac{\partial p}{\partial r}. \quad (2.9)$$

Here W denotes the flow relative to the solid per unit area, or filtration velocity, μ is the viscosity of the fluid and k is the permeability of the body, which will in general be strain dependent. Klachnar and Tarbell (1987) proposed the modelling the permeability of arterial tissue as an exponentially increasing function of the strain. Kaczmarek et al. (1997) suggested a small strain linear approximation between the inverse permeability and the strain. A model of either form introduces a material parameter which has unknown value, so in this work we keep the permeability constant and accept that one of the important elements of poroelasticity, linkage between the permeability and strain, must await better measurements of the physical properties of the parenchyma.

We shall also use the well known formula for steady flow of a Newtonian fluid through a rigid cylindrical pipe, or Poiseuille flow, so that

$$Q_a = \frac{\pi d^4}{128\mu L} (p_1 - p_2). \quad (2.10)$$

where Q_a is the volume of fluid flowing per unit time, d is the diameter of the pipe, L is the length of the pipe and p_1 and p_2 are the pressures at either end.

2.3 Geometry

We use a spherical geometry based on the first mechanical model for a realistic brain geometry proposed in Hakim et al. (1976). The brain is modelled as being composed of two concentric,

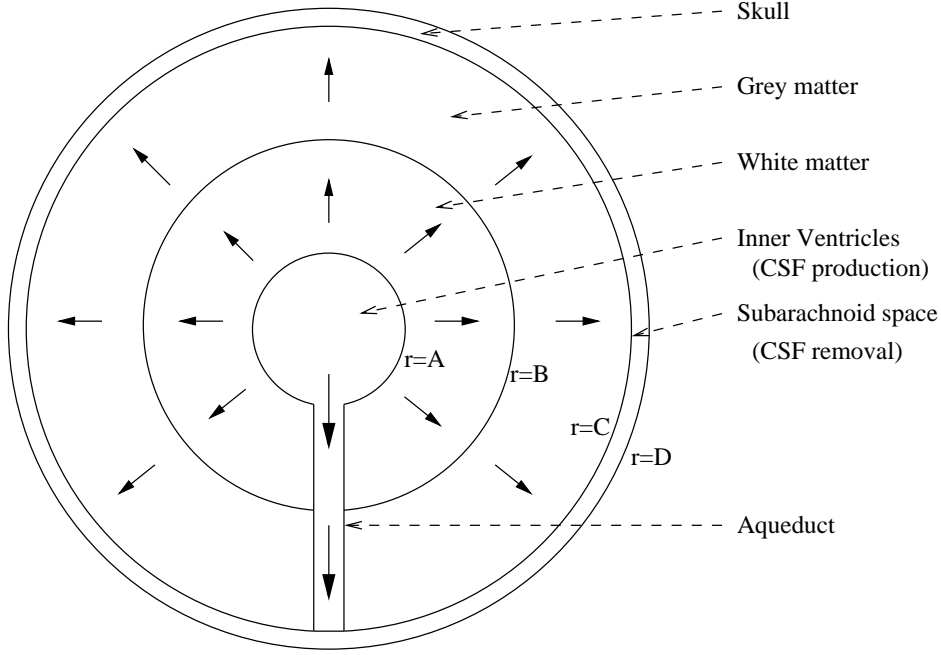


Figure 1: Schematic model of brain, showing inner ventricles, aqueduct, grey and white matter, subarachnoid space (assumed to have negligible thickness) and skull

porous, linearly elastic thick shells with outer radii B and C , which represent the white and grey matter respectively. Each layer may have different mechanical properties, reflecting the different properties of each type of tissue. The ventricles are modelled as a spherical cavity of radius A , located at the centre of the brain, while the Dura Matter, skull and scalp are represented by a single spherical layer of impermeable solid, outer radius D , enclosing the system. A narrow cylindrical channel (representing the aqueduct) of diameter d runs from the central ventricles to the interface between the grey matter and the skull (the subarachnoid space). We suppose that since the volume of this channel will be very small relative to the volume of the brain it will have no effect on the solid mechanical properties of the surrounding tissue.

The central cavity is filled with fluid (CSF) of viscosity μ which is produced at a constant rate Q_p . This fluid flows from the ventricles through the aqueduct and the porous tissue of the parenchyma into the subarachnoid space, where it is absorbed into the blood. This absorption is assumed to be proportional to the pressure difference between the blood and the CSF in the subarachnoid space. We expect that in the normal physiological state the vast majority of fluid transfer will occur through the aqueduct, as is observed *in vivo*. Should this flow be constrained as a result of stenosis of the aqueduct (so that the effective diameter of the aqueduct becomes small) we expect a much greater degree of flow through the brain itself, as happens in patients with hydrocephalus. In the case where a shunt is used to divert CSF into the bloodstream we suppose that fluid is removed directly from the ventricles at a rate Q_S .

The schematic geometry of our model is illustrated in figure 1, and while this represents a significant simplification of the make up of a real brain but we believe that it captures the key geometric and mechanical properties necessary for our purposes. In particular, there is some justification for the use of a spherical model of the ventricles (which in a healthy brain

are in fact narrow, ‘C-shaped’ cavities) by their approximately spherical configuration which is observed in hydrocephalus.

2.4 Material properties

Perhaps the most important decision to be made in modelling the material properties of the brain tissue involves the choice of constitutive equation for the solid matrix. It is well known that biological soft tissues rarely obey Hooke’s law but instead exhibit a mechanically nonlinear stress-strain relationship, see Sahay (1984) and Fung (1993). Some progress has recently been made in the formulation of such a non-linear model for the brain based on the theory of hyperelasticity (see Sahay et al. (1992), Miller and Chinzei (1997)). Sahay and Kothiyal (1984) even modelled the intracranial pressure-volume relationship in this fashion. They were, however, unable to reproduce the behaviour of the the brain under pressure, most likely because their model was unable incorporate the porous nature of the parenchyma. Indeed it seems that at present no theoretical basis for modelling a mechanically nonlinear poroelastic material exists. We therefore follow all of the previous authors in the field by using a Hookean form for the stress-strain behaviour of the brain, see equations (2.1). Since the white and grey matter may be in general be expected to exhibit different material properties we denote the Poisson’s ratios and Young’s moduli of each as ν_w and ν_g and E_w and E_g . As indicated above, the white and grey matter are taken to have constant permeability, k_w and k_g respectively.

The outer layer consisting of the dura matter, skull and scalp is taken to be homogenous with elasticity constants ν_s and E_s and zero permeability. While in reality each of the three components of this layer will exhibit distinct material properties, we justify our assumption of homogeneity by suggesting that only the comparatively very rigid skull is likely to be of mechanical significance. Since the grey matter and the outer layer of tissue are in contact in our model we suppose that the radial displacement and stress will be continuous at the interface ($r = C$). At the interface between the white and grey matter ($r = B$) we will need to impose the condition that the displacement, radial stress, fluid pressure and flow rate are all continuous.

2.5 Quasi-steady approximation

In formulating the governing equations for our model we shall consider only the quasi-steady behaviour of the system as the evolution of hydrocephalus occurs on a timescale of days and weeks (Hakim et al., 1976), inertial terms in the governing equations which represent the propagation of waves through the tissue are unlikely to affect the process of the brain settling into a hydrocephalic state. This conclusion is supported by the work of Stastna et al. (1998) who showed that the retention of such terms led to waves propagating on a time scale of order 10^{-2} s, much too short a time to affect the onset of the condition.

Thus by assuming changes happen slowly, we introduce time dependence to the behavior of the ventricle walls, the displacement of which will be of critical importance in the comparison of our results with clinical observations. We model the time rate of change of the volume of the ventricular cavity as being equal to the difference between the production rate of CSF and the total drainage rate through the aqueduct, parenchyma and any shunting device present, see equation (4.2). This will allow us to construct a phase plot of the behaviour of the ventricle wall, and hence to investigate the stability or otherwise of our steady state solutions. We will also be able to analyse how some variation in the material parameters affects the position

and stability of the steady state.

2.6 Onset and Treatments

We shall analyse the onset of hydrocephalus in three ways. Stenosis of the aqueduct, the main cause of the illness, can be modelled by reducing the value of the aqueduct diameter, d . We further simulate a) hydrocephalus caused by intraventricular infection or haemorrhage by varying the viscosity and b) hydrocephalus from impaired absorption in the subarachnoid space. We also wish to consider the effect of treatments, in particular shunting, on the mechanical behavior of the brain.

Using a phenomenological model for the quantitative properties of shunts based on the results recorded by Czosnyka et al. (1997) we suppose that the flow rate through the shunt, Q_S , driven by a pressure difference between the ventricle and the blood, $\Delta p = p_w(A, t) - p_{bp}$, takes the form

$$Q_S = \begin{cases} S_1 \Delta p & \text{for } \Delta p > 0, \\ 0 & \text{for } \Delta p \leq 0, \end{cases} \quad (2.11)$$

for ‘ball on spring’ devices and

$$Q_S = \begin{cases} S_2 \Delta p + S_3 \Delta p^2 & \text{for } \Delta p > 0, \\ 0 & \text{for } \Delta p \leq 0, \end{cases} \quad (2.12)$$

for shunts with silicone diaphragm valves. Here S_1 - S_3 are physical parameters which will depend on the material properties of the shunt, $p_w(A, t)$ is the CSF pressure in the ventricles and p_{bp} is the blood pressure.

Other methods of treating hydrocephalus can also be studied using the model. A surgical procedure to widen the aqueduct (the removal of a tumour, say) could be represented by increasing d after it had been constricted for some time. We shall use the quasi-steady model to study the effect of a lumbar puncture by instantaneously reducing the volume of the ventricles and observing how, or indeed if, they return to a steady configuration.

3 Hydro-elastic system of equations

3.1 Fluid

The continuity equation for spherical flow with velocity V of an incompressible fluid in a biphasic medium is

$$\frac{\partial \zeta}{\partial t} + \frac{1}{r^2} \frac{\partial}{\partial r} r^2 V + Q_{ab} = 0 \quad (3.1)$$

where flux can be decomposed in terms of the fluid velocity W and the matrix velocity u_t as

$$V = W + u_t.$$

Applying our assumptions of quasi-steady state and no CSF absorption in the brain, we have that the equilibrium equation for the fluid is simply

$$\frac{\partial W}{\partial r} + \frac{2W}{r} = 0.$$

Now we apply D’Arcy’s Law, (2.9), to express the filtration velocity in terms of the pressure and then split the domain into the white matter $A \leq r < B$ and grey matter $B \leq r < C$, so

that the governing equations for the fluid pressure in the white matter, p_w , and grey matter, p_g , are

$$\frac{\partial^2 p_w}{\partial r^2} + \frac{2}{r} \frac{\partial p_w}{\partial r} = 0 \quad A \leq r \leq B \quad (3.2)$$

and

$$\frac{\partial^2 p_g}{\partial r^2} + \frac{2}{r} \frac{\partial p_g}{\partial r} = 0 \quad B \leq r \leq C. \quad (3.3)$$

We do not include expressions for the pressure in the region $C \leq r \leq D$ since no fluid is present in that part of the domain.

3.2 Solid matrix equations

The governing equations for the solid phase are derived from the poroelastic equations for spherically symmetric deformation again assuming quasi-steady conditions.

The strains and the dilation is given in terms of the radial displacement, u , by

$$\epsilon_{rr} = \frac{\partial u}{\partial r}, \quad \epsilon_{\theta\theta} = \epsilon_{\phi\phi} = \frac{u}{r}, \quad \epsilon_{r\theta} = \epsilon_{\theta\phi} = \epsilon_{\phi r} = 0,$$

$$\varepsilon = \epsilon_{rr} + \epsilon_{\theta\theta} + \epsilon_{\phi\phi} = \frac{\partial u}{\partial r} + 2\frac{u}{r}.$$

Substituting these expressions in equation (2.5) leads to expressions for the stresses,

$$\begin{aligned} \sigma_{rr} &= E \left(\frac{1-\nu}{(1+\nu)(1-2\nu)} \right) \frac{\partial u}{\partial r} + \frac{2E\nu}{(1+\nu)(1-2\nu)} \frac{u}{r} - \alpha p, \\ \sigma_{\theta\theta} = \sigma_{\phi\phi} &= \frac{E\nu}{(1+\nu)(1-2\nu)} \frac{\partial u}{\partial r} + \frac{E}{(1+\nu)(1-2\nu)} \frac{u}{r} - \alpha p, \end{aligned} \quad (3.4)$$

$$\sigma_{r\theta} = \sigma_{\theta\phi} = \sigma_{\phi r} = 0.$$

Since there are no body forces and using the quasi-steady approximation, the stress is divergence free, giving

$$\frac{\partial \sigma_{rr}}{\partial r} + \frac{1}{r} (2\sigma_{rr} - \sigma_{\theta\theta} - \sigma_{\phi\phi}) = 0.$$

We now substitute expressions (3.4) into the above equation to find the governing equations for the displacement of the white matter u_w ,

$$\frac{\partial^2 u_w}{\partial r^2} + \frac{2}{r} \frac{\partial u_w}{\partial r} - 2\frac{u_w}{r^2} = E_w^* \frac{\partial p_w}{\partial r} \quad A \leq r \leq B, \quad (3.5)$$

and of the grey matter u_g ,

$$\frac{\partial^2 u_g}{\partial r^2} + \frac{2}{r} \frac{\partial u_g}{\partial r} - 2\frac{u_g}{r^2} = E_g^* \frac{\partial p_g}{\partial r} \quad B \leq r \leq C, \quad (3.6)$$

where

$$E_w^* = \alpha \frac{(1+\nu_w)(1-2\nu_w)}{E_w(1-\nu_w)} \quad \text{and} \quad E_g^* = \alpha \frac{(1+\nu_g)(1-2\nu_g)}{E_g(1-\nu_g)}.$$

We can simply perform the above analysis with $p = 0$ to find the governing equation for the displacement of the impermeable outer layer of tissue (the skull), u_s ,

$$\frac{\partial^2 u_s}{\partial r^2} + \frac{2}{r} \frac{\partial u_s}{\partial r} - 2 \frac{u_s}{r^2} = 0 \quad C \leq r \leq D. \quad (3.7)$$

We now have a set of governing equations (3.2)-(3.3) and (3.5)-(3.7) which describe the behaviour of the independent variables for pressure and displacement.

4 Boundary Conditions

We have one second order ordinary differential equation each governing the fluid pressure and the solid displacement in the white and grey matter and another for the displacement of the skull, giving a total of five second order equations. We therefore require ten boundary conditions in order to completely solve the system; four on the pressure/fluid velocity and six on the displacement/solid stress. We apply two boundary conditions at the ventricle wall ($r = A$), four at the interface between the white and grey matter ($r = B$), three at the interface of the grey matter and the skull ($r = C$) and one at the outer surface of the skull ($r = D$).

4.1 Ventricles

The boundary condition for the pressure in the ventricles, $p_w(A, t)$, is the most complicated and perhaps the most important which we shall apply. It is here where we incorporate the flow of fluid through the aqueduct and shunting into the model. The deformation of the ventricles is also the clearest clinical sign of hydrocephalus, so the size of the radial deformation of the ventricle wall, $u_w(A, t)$, will be critical in evaluating the model.

If we are considering a steady state situation, variables are independent of time and since the volume of CSF being produced must be equal to the volume of fluid flowing out,

$$\overbrace{\frac{\pi d^4}{128 \mu L} [p_w(A) - p_g(C)]}^1 - \overbrace{4 \pi A^2 \frac{k_w}{\mu} \frac{\partial p_w}{\partial r} \Big|_{r=A}}^2 + \overbrace{S(p_w(A))}^3 = \overbrace{Q_p}^4. \quad (4.1)$$

The first term models the flow of fluid through the aqueduct, Q_a , driven by the pressure difference between the ventricles and the subarachnoid space $[p_w(A) - p_g(C)]$, and d and L represent an effective diameter and length of the aqueduct respectively, see (2.10). If the aqueduct is being forced into collapse then it will not remain cylindrical but its length will not change much so we continue to use a Poiseuille flow approximation but interpret d as the diameter of a cylindrical tube with the same flow rate for a given pressure drop. The second term models the flow of fluid across the ventricle wall into the parenchyma using the velocity of the flow from D'Arcy's law (2.9). The third term is the flow rate through any shunt and the fourth term, is the production rate of fluid, assumed constant. If now we invoke a quasi-steady approximation and allow the ventricle radius to vary slowly we incorporate this time dependence by introducing a term \dot{V} , the rate of change of the ventricular volume with respect to time. Thus we have

$$\dot{V} = Q_p - \frac{\pi d^4}{128 \mu L} [p_w(A, t) - p_g(C, t)] + 4 \pi A^2 \frac{k_w}{\mu} \frac{\partial p_w}{\partial r} \Big|_{r=A} - S(p_w(A, t)). \quad (4.2)$$

Now expressing the ventricular volume in terms of the initial radius A and the deformation of the ventricle, $u_w(A, t)$,

$$\dot{V} = \frac{d}{dt} \left[\frac{4}{3} \pi (A + u_w(A, t))^3 \right].$$

Substituting into (4.2) we have a first order non-linear differential equation for $u_w(A, t) \equiv u_A(t)$,

$$\begin{aligned} \frac{du_A}{dt} = \frac{1}{4\pi(u_A(t) + A)^2} & \left[Q_p - \frac{\pi d^4}{128\nu L} [p_w(A, t) - p_g(C, t)] \right. \\ & \left. + 4\pi A^2 \frac{k_w}{\mu} \frac{\partial p_w}{\partial r} \Big|_{r=A} - S(p_w(A, t)) \right]. \end{aligned} \quad (4.3)$$

The second boundary condition to be applied here refers to the solid matrix. Since the brain is untethered at the ventricle wall we assume that the radial stress in the solid,

$$\sigma'_{rr} = \sigma_{rr} + \alpha p,$$

is zero at its boundary. Hence our second boundary condition is

$$E_w \left(\frac{1 - \nu_w}{(1 + \nu_w)(1 - 2\nu_w)} \right) \frac{\partial u_w}{\partial r} \Big|_{r=A} + \frac{2E_w \nu_w}{(1 + \nu_w)(1 - 2\nu_w)} \frac{u_w(A, t)}{A} = 0. \quad (4.4)$$

4.2 Interface of White and Grey Matter

The four boundary conditions to be applied at $r = B$ all come from the continuity of physical quantities in our model; the displacement, radial stress, fluid pressure and filtration velocity must all be continuous. Hence we match displacements

$$u_w(B, t) = u_g(B, t) \quad (4.5)$$

and stresses

$$\begin{aligned} E_w \left(\frac{1 - \nu_w}{(1 + \nu_w)(1 - 2\nu_w)} \right) \frac{\partial u_w}{\partial r} \Big|_{r=B} + \frac{2E_w \nu_w}{(1 + \nu_w)(1 - 2\nu_w)} \frac{u_w(B, t)}{B} - \alpha p_w(B, t) \\ = E_g \left(\frac{1 - \nu_g}{(1 + \nu_g)(1 - 2\nu_g)} \right) \frac{\partial u_g}{\partial r} \Big|_{r=B} + \frac{2E_g \nu_g}{(1 + \nu_g)(1 - 2\nu_g)} \frac{u_g(B, t)}{B} - \alpha p_g(B, t) \end{aligned} \quad (4.6)$$

in the solid. Note that since the αp terms will cancel from each side of the equation it does not matter whether we choose to equate the effective stresses $\sigma'_{rr}(B)$ or total stresses $\sigma_{rr}(B)$.

We also match fluid pressures

$$p_w(B, t) = p_g(B, t) \quad (4.7)$$

and filtration velocities

$$-\frac{k_w}{\mu} \frac{\partial p_w}{\partial r} \Big|_{r=B} = -\frac{k_g}{\mu} \frac{\partial p_g}{\partial r} \Big|_{r=B} \quad (4.8)$$

across the interface.

4.3 Subarachnoid Space

The first two boundary conditions at $r = C$ are a result of the continuity of the behaviour of the solid between the brain and the skull. Thus we apply continuity of displacements

$$u_g(C, t) = u_s(C, t) \quad (4.9)$$

and stresses

$$\begin{aligned} E_g \left(\frac{1 - \nu_g}{(1 + \nu_g)(1 - 2\nu_g)} \right) \frac{du_g}{dr} \Big|_{r=C} + \frac{2E_g\nu_g}{(1 + \nu_g)(1 - 2\nu_g)} \frac{u_g(C)}{C} - \alpha p_w(C, t) \\ = E_s \left(\frac{1 - \nu_s}{(1 + \nu_s)(1 - 2\nu_s)} \right) \frac{du_s}{dr} \Big|_{r=C} + \frac{2E_s\nu_s}{(1 + \nu_s)(1 - 2\nu_s)} \frac{u_s(C, t)}{C} \end{aligned} \quad (4.10)$$

is a similar way to those at the interface of the white and grey matter.

The third boundary condition relates to the absorption of fluid which occurs in the subarachnoid space. Modelling the absorption as proportional to the pressure difference between the CSF and the blood stream, we have that

$$\frac{p_g(C, t) - p_{bp}}{R\mu} = \frac{\pi d^4}{128\mu L} [p_w(A, t) - p_g(C, t)] - 4\pi C^2 \frac{k_g}{\mu} \frac{\partial p_g}{\partial r} \Big|_{r=C}. \quad (4.11)$$

The term on the left hand side of this equation refers to the flow of fluid through the arachnoid villi, which is driven by the pressure difference ($p_g(C) - p_{bp}$) and where R is a parameter which models the resistivity of the villi to flow. Note that since flow cannot occur from the blood into the subarachnoid space we implicitly assume that in all cases $p_g(C) \geq p_{bp}$.

4.4 Skull

The last boundary condition applies to the outside of the skull, $r = D$. Here we simply assume that the solid is untethered and hence stress free so that

$$E_s \left(\frac{1 - \nu_s}{(1 + \nu_s)(1 - 2\nu_s)} \right) \frac{du_s}{dr} \Big|_{r=D} + \frac{2E_s\nu_s}{(1 + \nu_s)(1 - 2\nu_s)} \frac{u_s(D, t)}{D} = 0. \quad (4.12)$$

The total stress and effective stress are identical here since there is no fluid pressure, hence there is no need to make any distinction between them in applying this boundary condition.

4.5 Solution method

The formulation we have derived provides us with a set of ten boundary conditions, (4.1) or (4.2) and (4.4)-(4.12) with which to solve the governing equations (3.2)-(3.3) and (3.5)-(3.7). The spherical geometry allows the pressure and displacement to be determined in terms of simple powers or the radial distance and unknown constants. In the steady case the solutions, when substituted into the boundary conditions, these reduce to solving a 10×10 linear system for the unknown constants. This has been done using *Maple* to solve the linear system analytically. In the unsteady case, the nine boundary conditions (4.4)-(4.12) are applied leaving just the ventricle displacement undetermined. Equation (4.3) can then be solved numerically using *MATLAB* to provide the time evolution of the deformation of the ventricle wall and corresponding stress and displacement within the grey and white matter, for full details see Smillie (2003). In addition to following the time evolution, we also use a phase plot of u_A vs. $\frac{du_A}{dt}$ to determine the stability of a steady state solution to the model.

5 Parameter Estimation

The evaluation of the material parameters is often a non-trivial problem in biomechanics since the usual engineering tests used to measure the physical properties of a material are often difficult to apply to soft biological tissue. There is also the question of different material behaviour *in vivo* and *in vitro*, with experimentation in the former case being ethically as well as practically problematic. In the following section we shall therefore attempt to estimate numerical values for all of the parameters in our model, but some will inevitably be rough approximations.

5.1 Geometry of the Brain

Since the spherically symmetric geometry of the brain in the model is an idealization we must calculate values for A, B, C, D, L and d which are in some sense equivalent to those in the real geometry. We use values for the radii of the ventricles, white matter and grey matter which approximately correspond to their location in the adult male brain Kaczmarek et al. (1997). Hence we have that the ventricles are of radius $A = 3 \times 10^{-2}\text{m}$, the interface of the white and grey matter is at $B = 7 \times 10^{-2}\text{m}$ and the the brain itself has radius $C = 10 \times 10^{-2}\text{m}$. Taking that the skull to be of thickness 0.2 cm (Drossos et al., 2000), the outer layer of the model will be of radius $D = 10.2 \times 10^{-2}\text{m}$.

The diameter of a healthy cerebral aqueduct varies along its length and between individuals, we use the average value reported in Bickers and Adams (1949), $d = 4 \times 10^{-3}\text{m}$. Since we have assumed that the aqueduct is straight and runs from the ventricles to the subarachnoid space we suppose that it is of length $L = C - A = 7 \times 10^{-2}\text{m}$.

5.2 Poroelastic constants

The poroelastic constants are perhaps the most difficult class of parameters for which to find numerical values. Kaczmarek et al. (1997) use a value of $E = 1 \times 10^4\text{N/m}^2$ for the Young's modulus, taken from Metz et al. (1970). As was noted in Levine (1999) however, this represents the instantaneous, or undrained, value of the coefficient, the drained value is likely to be somewhat smaller. It is also unclear whether the value of the Poisson's ratio used, $\nu = 0.35$, was measured under drained or undrained conditions.

In formulating a model of the brain all of the previous authors have assumed that the brain perfectly saturated so that $\alpha = \beta = 1$. In order to enable us to convert from undrained to drained elastic moduli we instead suppose that the brain is almost but not perfectly saturated with fluid, and use the values given in Wang (2002) for such a mixture,

$$\alpha = 1 \quad \text{and} \quad \beta = 0.99.$$

Now, if the value of ν quoted above refers to drained conditions then, using equation (2.7), we have that the undrained Poisson's ratio is

$$\nu_u = 0.4983,$$

that is, the mixture is virtually incompressible under undrained conditions. This may explain why Nagashima *et al* erroneously used a value of $\nu = 0.4999$ in their model of the hydrocephalic

brain. Given an undrained Young's modulus of $E_u = 1 \times 10^4 \text{N/m}^2$ and inverting the second of equations (2.7) we have a value of the drained Young's modulus

$$E = \frac{1 - 2\nu}{1 - 2\nu_u} E_u (1 - \alpha\beta) = 0.9010 \times 10^4 \text{N/m}^2,$$

only a little lower than the value used by Kaczmarek *et al.*

However, if the value of the Poisson's ratio used in Kaczmarek *et al.* (1997) was measured under undrained conditions (so that $\nu_u = 0.35$), we have that the drained value of the Poisson's ratio is

$$\nu = \frac{3\nu_u - \alpha\beta(1 + \nu_u)}{3 - 2\alpha\beta(1 + \nu_u)} = -0.8761,$$

a value of ν which is unusual, but not physically inadmissible. Materials with negative Poisson's ratio exist and are thought to occur in other places in the body, see for example Lakes (1993), Lakes (2002) so while the suggestion of a negative Poisson's ratio for brain tissue is highly unusual, it is not an impossible suggestion. Again assuming that $E_u = 1 \times 10^4 \text{N/m}^2$, we then have a Young's modulus of

$$E = 0.9177 \times 10^3 \text{N/m}^2,$$

an order of magnitude lower than that used by Kaczmarek *et al.* One of the main weaknesses of their model was the unrealistically high levels of intraventricular pressure ($\sim 40 \text{kPa}$) required to maintain displacements of the ventricle wall consistent with those observed in hydrocephalus. A significantly lower value of E might resolve this discrepancy, therefore we shall consider these values of the elastic constants as being potentially viable despite the unusual form of ν . Since the value of ν has to be something of an open question we present results for both of the above scenarios ($\nu = 0.35$ and $\nu_u = 0.35$) and compare the results.

The above results were measured using a section of brain composed mainly of white matter. In the absence of any quantitative data regarding different elastic properties of the grey matter we shall assume that $E_w = E_g = E$ and $\nu_w = \nu_g = \nu$ when computing our results, though in reality it is likely that the grey matter will be a little more rigid. For the skull we use values of

$$E_s = 1 \times 10^9 \text{N/m}^2 \quad \text{and} \quad \nu_s = 0.3,$$

from van Rietbergen *et al.* (1995).

In order to fully characterize the poroelastic behaviour of the brain we require numerical values for the permeabilities k_w and k_g . Kaczmarek *et al.* calculated the permeability of the brain using the results of Reulen *et al.* (1977), however the value given as 'permeability' in their paper is actually the permeability scaled with fluid viscosity. Based on their calculations the appropriate values for the permeabilities of the white and grey matter are

$$k_w = 1.426 \times 10^{-14} \text{m}^2 \quad \text{and} \quad k_g = 1.426 \times 10^{-16} \text{m}^2 \quad \text{respectively.}$$

5.3 Fluid Flow and Drainage

The physical properties of the CSF system itself are rather better documented. Since CSF has physical properties similar to water we assume that it has dynamic viscosity (Fay, 1994)

$$\mu = 8.91 \times 10^{-4} \text{Ns/m}^2.$$

The production rate of CSF in the ventricles is reported to be (Bradbury, 1993)

$$Q_p = 5.833 \times 10^{-9} \text{m}^3/\text{s},$$

which we take to be independent of intraventricular pressure. We may now compare the relative importance of the aqueduct and the porous brain in draining fluid from the ventricles. Taking a typical length scale of L and pressure scale of P and dividing term 1 of equation (4.1) by term 2 gives

$$\frac{\pi d^4 P / 128 \mu L}{4 \pi A^2 k_w P / \mu L} \approx 1750.$$

Thus, in a healthy brain, flow through the aqueduct accounts for virtually all of the transfer of CSF through the ventricular system. Only in a pathological state, for example when $d \rightarrow 0$, will a significant proportion of flow occur through the parenchyma. We therefore have that a typical flow speed in the aqueduct is

$$U = \frac{4Q_p}{\pi d^2} = 1.16 \times 10^{-4} \text{m/s}.$$

Then, given a kinematic viscosity $\mu/\rho = 8.91 \times 10^{-7} \text{m}^2/\text{s}$, we have that the Reynolds number for flow in the aqueduct is

$$\text{Re} = \frac{\rho U L}{\mu} \approx 10^{-1}.$$

To evaluate R , the resistance of the arachnoid villi, we suppose that the resistance is such that the rate of outflow is exactly equal to the CSF production rate Q_p for the normal physiological value of $p(A) - p_{\text{bp}} = 441 \text{ N/m}^2$. Hence

$$R = \frac{[p(A) - p_{\text{bp}}]_{\text{norm}}}{\mu Q_p} = 8.490 \times 10^{13} \text{m}^{-3}.$$

We assume a typical value for venous blood pressure of 100 mmHg or $p_{\text{bp}} = 1.333 \times 10^4 \text{N/m}^2$.

In order to determine values for S_1 , S_2 and S_3 , the parameters governing flow through a shunt, we use a least squares fit to the data in Czosnyka et al. (1997) to give that $S_1 = 1.253 \times 10^{-10} \text{m}^5/\text{Ns}$, $S_2 = 3.031 \times 10^{-11} \text{m}^5/\text{Ns}$ and $S_3 = 3.766 \times 10^{-14} \text{m}^7/\text{N}^2\text{s}$.

6 Results

We now consider solutions of the model to test against clinical observations and to examine the behaviour of the response of the brain to a variation in these parameters. The major indicators we consider are the displacement of the ventricle wall, $u_w(A, t)$, and the intraventricular pressure, $p_w(A, t)$, since these are the key clinical signs of hydrocephalus. The ventricular aspect ratio,

$$\Gamma = \frac{C + u_g(C, t)}{A + u_w(A, t)},$$

was introduced by Hakim et al. (1976) as an alternative measure of the extent of hydrocephalus, we shall use it when making a comparison with the results of those authors. We shall also use the notion of the magnitude of the shear stress

$$|\tau(r, t)| = \frac{|\sigma_r(r, t) - \sigma_\theta(r, t)|}{2}$$

as measure of tissue damage, see Holbourn (1943). A summary of parameter values is given in table 1.

A	3×10^{-2} m	E (Case 1)	9.010×10^3 N/m ²
B	7×10^{-2} m	E (Case 2)	9.177×10^2 N/m ²
C	10×10^{-2} m	ν (Case 1)	0.35
D	10.2×10^{-2} m	ν (Case 2)	-0.8761
L	7×10^{-2} m	E_s	1×10^9 N/m ²
d	4×10^{-3} m	ν_s	0.3
α	1	Q_p	5.833×10^{-9} m ³ /s
β	0.99	μ	8.91×10^{-4} Ns/m ²
k_w	1.426×10^{-14} m ²	R	8.490×10^{13} m ⁻³
k_g	1.426×10^{-16} m ²	p_{bp}	1.330×10^4 N/m ²

Table 1. Values of physical constants used to calculate model solutions.

6.1 Severe Hydrocephalus

We begin by solving the model for the case of complete occlusion of the aqueduct, $d = 0$, and no shunt, $Q_S = 0$. In this case it is to be expected that the intraventricular pressure will be significantly above normal physiological values, since all of the CSF produced in the ventricles must be driven through the parenchyma, a much more resistant pathway than the aqueduct. This pressure rise will induce a deformation in the parenchyma, the defining symptom of hydrocephalus.

Setting $d = 0$ is also a useful starting point since the results from this configuration of the model can be compared not only with clinical observations of severe hydrocephalus, but also with the other mathematical models of this condition (for example Kaczmarek et al. (1997) and Tenti et al. (1998)).

6.1.1 Flow and Pressure Distribution of CSF

In figure 2 we show the excess in pore pressure over the venous blood pressure. The intraventricular pressure, $p_w(A)$ is around 13 kPa above b.p. This value is rather higher than that typically observed clinically (CSF pressures in excess of 2 kPa above b.p. are usually considered abnormal) but is likely to be within the upper end of recorded hydrocephalic ventricular pressures. It is certainly closer to physiological levels than the intraventricular pressures in excess of 40 kPa predicted by the model of Kaczmarek *et al.*

The pressure falls off relatively slowly through the white matter ($A \leq r \leq B$) then drops much more sharply in the grey matter region of the brain ($B \leq r \leq C$), due to the lower permeability here. The step change in the gradient of fluid pressure at the interface is not physiological, its presence is due to our assumption that the brain can be divided into distinct regions of white and grey matter. In reality both tissue types are found throughout the parenchyma, with grey matter becoming more prevalent towards the periphery. A model in which the permeability is a monotonically decreasing function of radius may resolve this difficulty, though would of course lead to a different form of the solutions.

In steady state the volume of fluid flowing out through the arachnoid villi and into the bloodstream is constant, regardless of whether the fluid has arrived in the subarachnoid space via the aqueduct or the parenchyma. This means that in our model, as a consequence of

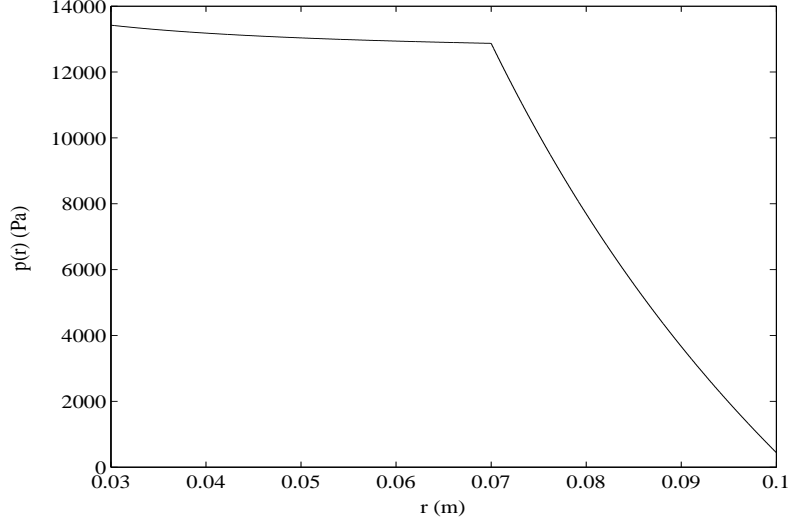


Figure 2: Fluid pressure in the white and grey matter

equation (4.11), the pressure in the subarachnoid space $p_g(C)$ will be always be relatively close to blood pressure. We were unable to find any empirical data on the fluid pressure in the subarachnoid space in hydrocephalic patients (probably due to the difficulty of performing such measurements), so it is difficult to assess the validity of this result.

Figure 3 shows the filtration velocity decreasing as the square of the radius. This is expected since no fluid is absorbed as it passes through the brain, hence the volume of fluid flowing through any given spherical surface should be constant. The filtration velocity is much higher in this case than the typical flow speed calculated in section 5.3. As the volume of CSF has risen, the residence time for the CSF will be greater but the time spent in the parenchyma will be less and such a change may have further consequences for the brain if the CSF plays a role in transferring nutrients from the ventricles to the subarchnoid space through the parenchyma.

6.1.2 Displacements and Stresses through the Brain

The elasticity constants E and ν are critical in determining the behaviour of the solid components of the brain. As explained above, we have calculated solutions for two values of Poisson's ratio, one positive (case 1) and one which is negative (case 2), and consequentially of uncertain applicability.

The radial displacement of the brain in both cases is shown in figure 4, where case 1 refers to ($\nu = 0.35, E = 9.010 \times 10^3 \text{ N/m}^2$), while case 2 has ($\nu = -0.8761, E = 9.177 \times 10^2 \text{ N/m}^2$). The displacement of the ventricle wall $u_w(A)$, which we shall consider to be the result most indicative of the extent of hydrocephalus, is in both cases around 0.012 m, while the outer surface of the brain experiences virtually no deformation, a consequence of the relatively rigid nature of the skull. This gives a ventricular aspect ratio of

$$\frac{C + u_g(C)}{A + u_w(A)} = 2.38,$$

which is close to the value of 2 given in Hakim et al. (1976) for a typical case of adult hydrocephalus.

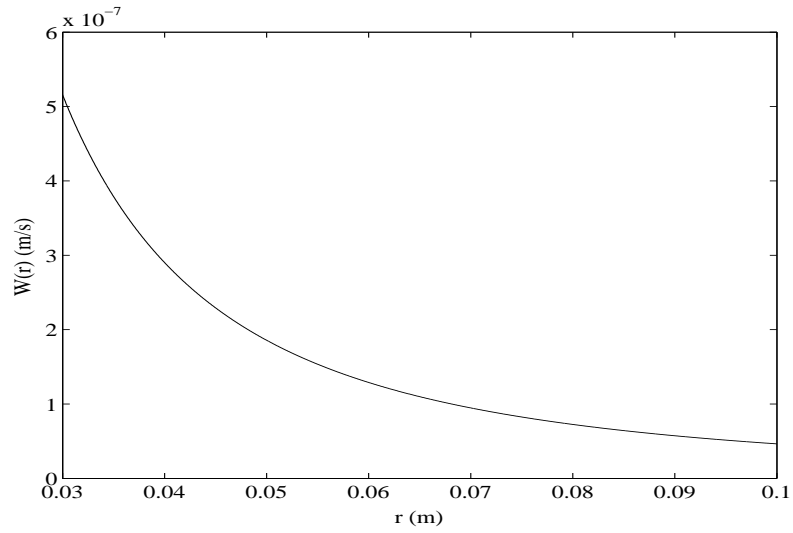


Figure 3: Filtration velocity (superficial) in the white and grey matter

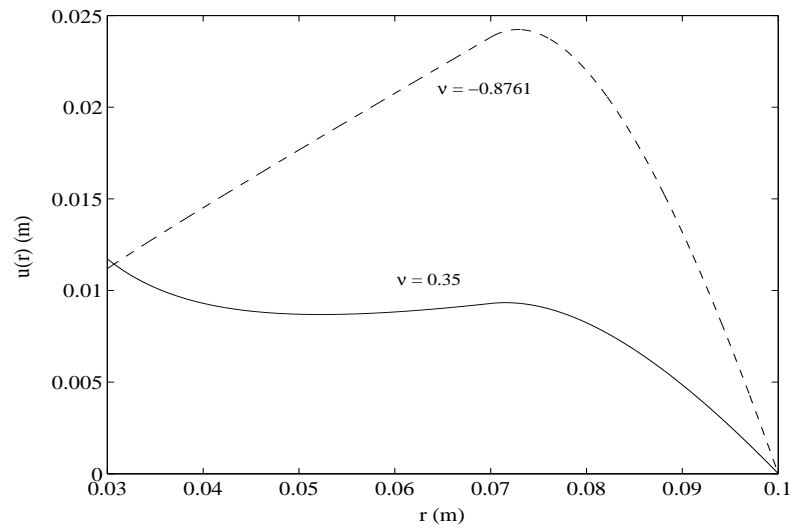


Figure 4: Radial displacement of tissue in white and grey matter for the two cases: $\nu = 0.35$ (—) and $\nu = -0.8761$ (- -)

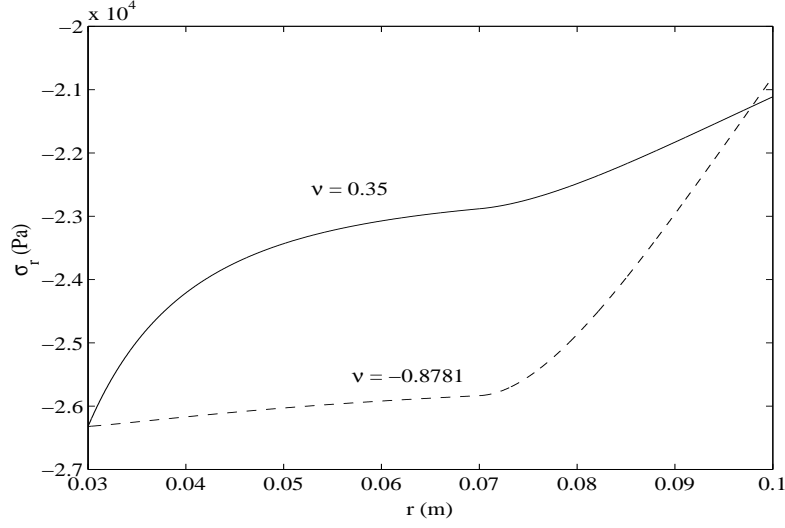


Figure 5: Radial stress for the two cases: $\nu = 0.35$ (—) and $\nu = -0.8761$ (- - -).

While the displacements of the outer and inner boundaries of the skull are similar for both sets of elastic constants the deformation through the brain is very different. In case 1 the deformation of the white matter is relatively constant, while in case 2 the deformation becomes larger away from the ventricles. This latter type of behaviour is not physiological, suggesting that the elastic parameters in this case are unlikely to be valid. The slight increase in the displacement as r approaches B in case 1 is also probably not physiological, this is again a consequence of our assumption that the brain can be divided into two distinct regions of white and grey matter. The results for the displacement in Case 1 are similar to those in Kaczmarek et al. (1997).

The radial stress distributions are shown in figure 5. The negativity of the total stresses in both cases 1 and 2 indicates that the stresses are compressive in nature. The stress falls quickly through the skull to the stress free outer surface of the head, again a consequence of the relative rigidity of the skull. For clarity we have omitted this from the figure since such a large change makes the stress distribution through the brain less clear.

The total stress at the ventricle wall is equal and opposite to the fluid pressure (including blood pressure) at this point. Since the solid parenchyma is untethered at the ventricle wall (4.4), it is the the pressure gradient in the fluid alone which induces the compression of the brain. In contrast to this, the magnitude of the total stress at the outer edge of the parenchyma is much greater then the fluid pressure and the stress there is largely due to the skull constraining the brain.

Since the solid exhibits unphysiological behaviour in case 2 we believe that the elastic parameters used in that case are not physiological, with the value of -0.8761 for the Poisson's ratio being the most likely cause of such unrealistic results. For the remainder of this report we shall therefore assume that

$$E = 9.010 \times 10^3 \text{N/m}^2 \quad \text{and} \quad \nu = 0.35.$$

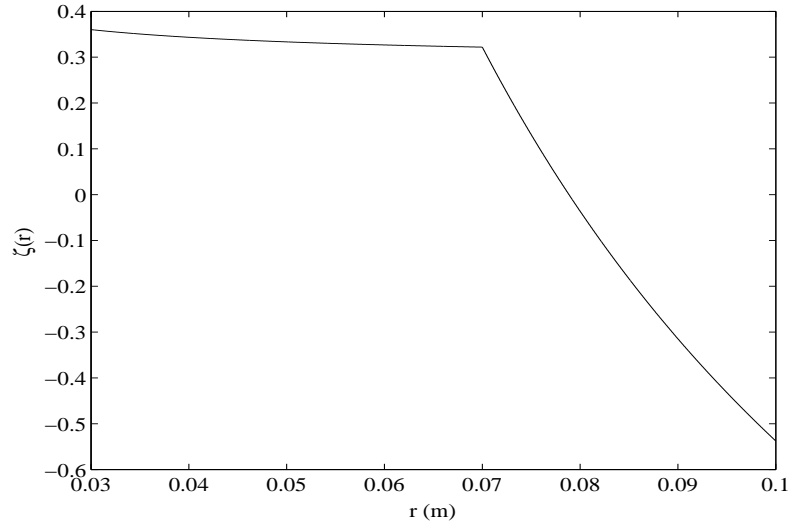


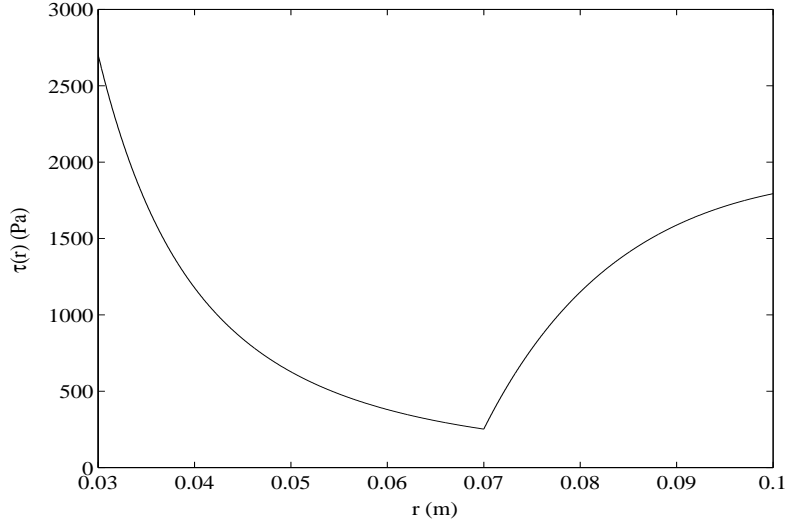
Figure 6: Increment of fluid content, $\nu = 0.35$

6.1.3 Effects on the Brain

Most of the damage to the tissue of the brain, and hence most of the symptoms of hydrocephalus, occur as the result of a combination of oedema and shear stresses in the solid. The increment of fluid content may be regarded as a measure of the former, see figure 6. Notice how the increase in fluid content is largely confined to the white matter and is most pronounced in the regions adjacent to the ventricle wall. This is in agreement with the clinical observations of oedema in hydrocephalus. In the areas of grey matter close to the subarachnoid space ζ becomes negative, indicating that in this region fluid has been squeezed out of the brain. Given that most of the compression of the parenchyma occurs in this region this seems like reasonable behaviour, and is supported by clinical evidence from CT scans of hydrocephalic patients (Kaczmarek et al., 1997).

Note that since we have assumed that the brain is almost completely saturated with fluid, hence $\alpha = 1$ and $\beta = 0.99$, we have from equation (2.6) that the increment of fluid content, $\zeta(r)$, is approximately the same as the dilation, $\varepsilon(r)$. This indicates that close to the ventricles the solid matrix expands, while in the peripheral regions it is compressed against the skull.

The magnitude of the shear stresses are plotted in figure 7. These indicate that in our model the most significant tissue damage takes place in the white matter adjacent to the ventricles and in the grey matter near the skull. As normal there is a step change in the nature of the solution at the interface of the white and grey matter, in this case the minimum amount of damage takes place here. The increased level of tissue damage at the periphery of the brain is in contrast to the results of Levine (1999), who found that shear stress decreased monotonically from a maximum at the ventricle wall. The high degree of compression of this region of the brain observed in hydrocephalus would suggest however that significant levels of damage may occur here, and hence our results may indicate a real physiological effect, rather than a mathematical anomaly caused by the simplified geometry employed in formulating the model.

Figure 7: Shear stress, $\nu = 0.35$

6.2 Onset of Hydrocephalus

One of the main advantages of our model is that it allows simulation of some of the causes of hydrocephalus by varying material parameters. First, we shall consider the effect of stenosis of the aqueduct, the most frequent cause of the condition, by reducing the value of d . Second, we model impaired absorption in the subdural space by increasing R and third, we consider variation in the viscosity of the CSF.

6.2.1 Stenosis of the Aqueduct

The dependence of the intraventricular pressure and ventricle wall displacement on the width of the aqueduct is shown in figure 8. It is clear that the system is resistant to even a relatively large decrease in d with little discernible effect so long as $d > 0.8 \times 10^{-3}$ m, a fifth of its physiological value. Once d drops below that value the effect on the brain is pronounced, with a large increase in intraventricular pressure, $p_w(A)$, and wall displacement, $u_w(A)$ as the effective aqueduct radius, d , approaches zero. Note that the pressure and the displacement tend to the equilibrium values determined for complete blockage of the aqueduct. The sensitivity of the model to changes in the diameter of the aqueduct below 0.8×10^{-3} m is a result of the d^4 term which appears in boundary conditions (4.1) and (4.11). This reinforces the view that complete occlusion of the cerebral aqueduct is the main cause of hydrocephalus.

We may model the effect of aqueduct stenosis on the time evolution of the system using the ventricular pressure boundary condition (4.2). In particular the stability of steady state solutions is illustrated in figure 9 by a phase plane diagram of $u_w(A)$ against $\frac{du_w(A)}{dt}$ for a range of values of d . The phase diagram is shown for three cases; complete occlusion of the aqueduct, $d = 0$ m, major occlusion of the aqueduct, $d = 0.25 \times 10^{-3}$ m, and minor occlusion of the aqueduct, $d = 1 \times 10^{-3}$ m. The steady state for the complete obstruction of the aqueduct is located at $u_w(A) = 0.012$ m, corresponding to the deformation state described in the previous section, while for the aqueduct open the steady state is located at the origin, corresponding to the undeformed configuration of the brain (the phase plot for $d = 4 \times 10^{-3}$ m, its physiological

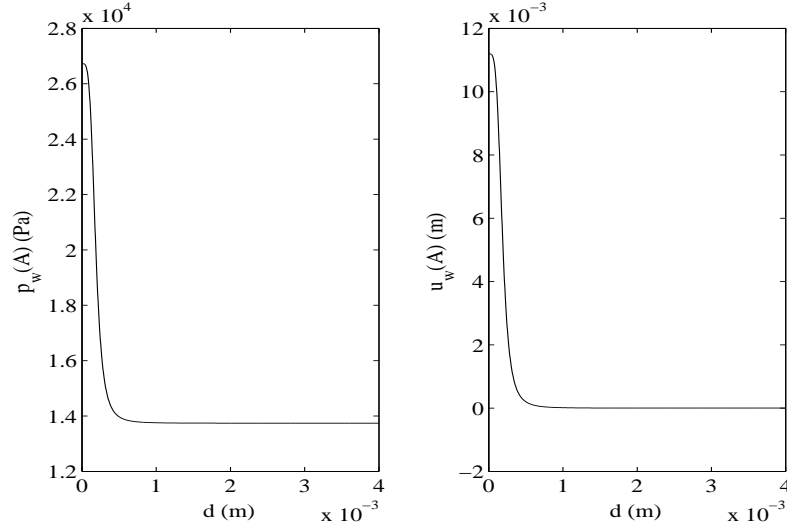


Figure 8: Effect of varying the aqueduct radius, d , on the ventricular pressure, $p_w(A)$, and wall displacement, $u_w(A)$

value, is very similar to that for $d = 1 \times 10^{-3}$ m, only with an even steeper gradient). When $d = 0.25 \times 10^{-3}$ m the deformation state is located between these two extremes.

All of the steady states are stable in nature. This has important consequence for the behaviour of the brain in both healthy and pathological conditions. In the healthy state the ventricles will return to their undeformed configuration (that is $u_w(A) = 0$) even if they are instantaneously subject to a large deformation, due to blow to the head for example. In the pathological state the ventricles will return to a deformed configuration even if their volume is temporarily reduced by treatment. Unless either d can be increased, by surgery to remove a tumour for example, or a permanent alternative drainage pathway can be constructed, for example by shunting, fluid will continue to be driven through the parenchyma with the consequent rise in intraventricular pressure and deformation of the brain.

The relatively steep gradient of the phase plot in the case of the open aqueduct indicates that the brain will quickly return to steady state after being perturbed, while the shallower gradients when $d = 1 \times 10^{-3}$ m and $d = 0$ mean that this configuration will recover more slowly.

We are able to plot the time evolution of hydrocephalus by solving the differential equation for the deformation of the ventricles (4.3) numerically, the results are shown in figure 10. In formulating these solutions we assumed that the aqueduct was completely blocked and used the initial condition

$$u_w(A, 0) = 0,$$

that is that the brain is initially in its undeformed state. Both the displacement of the ventricles and the intraventricular pressure approach their steady state values asymptotically. The time scale over which the onset of hydrocephalus occurs, 2.5×10^5 s \approx 3 days, is within the range of ‘days and weeks’ given by Hakim et al. (1976) as typical for the development of the condition.

6.2.2 Impaired absorption of CSF

We now consider potential alternatives to stenosis of the aqueduct as a cause of hydrocephalus. One such alternative is impaired absorption of fluid in the subarachnoid space, which in our

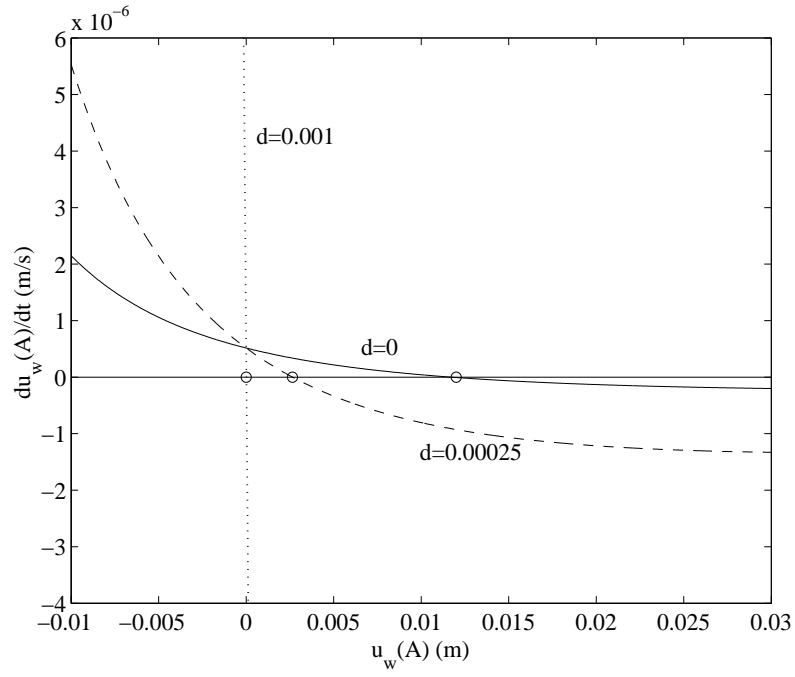


Figure 9: Phase plots for the wall displacement, $u_w(A, t)$ showing a stable fixed point (circled) for various aqueduct diameter: $d = 0$ (—), $d = 0.00025$ (- - -), $d = 0.001$ (···)

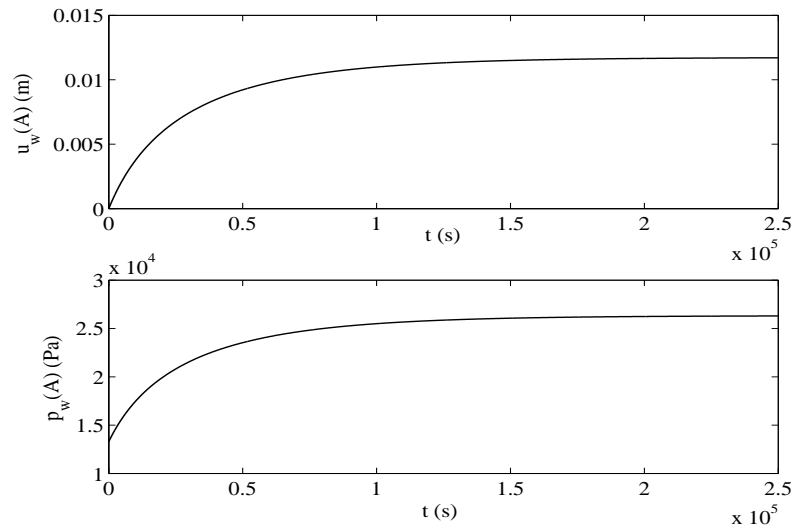


Figure 10: Time evolution of the ventricular pressure, $p_w(A, t)$, and wall displacement, $u_w(A, t)$ for severe hydrocephalus following a sudden blockage of the aqueduct

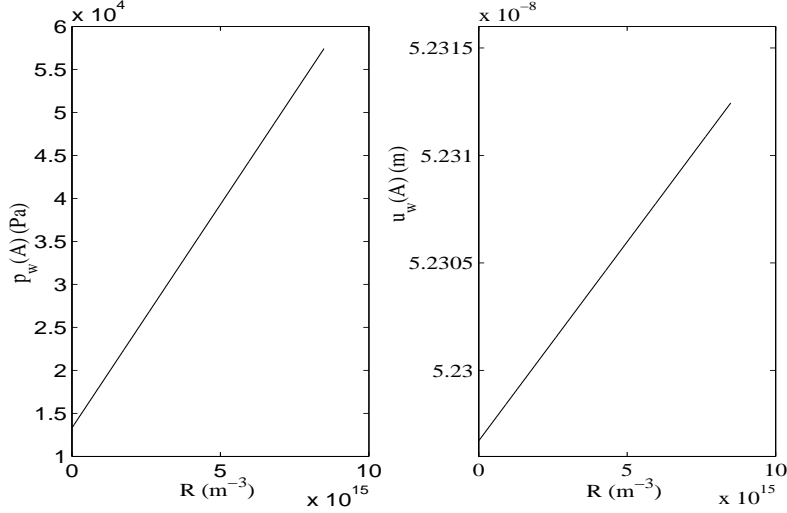


Figure 11: Effects of increasing the absorption resistance, R , on the ventricular pressure, $p_w(A)$, and wall displacement, $u_w(A)$

model should correspond to an increase in R , the resistivity of the arachnoid villi. Figure 11 shows the effect on the intraventricular pressure and displacement of increasing R by up to two orders of magnitude. Both plots show a linear dependence on the resistance, but the change in the magnitude of the pressure is much greater than the infinitesimal increase in the displacement. Given that it is a pressure increase in the ventricles which causes hydrocephalus such an effect seems difficult to explain. However it is not the fluid pressure which is the cause of the deformation but the pressure gradient, evident from the presence of only the derivative of p in equations (3.5) and (3.6). An increase in R means that the fluid pressure rises *throughout* the brain and ventricular system and so does not induce a deformation in the parenchymal matrix. Thus, in our model, an increase in the resistance of the arachnoid villi will not cause hydrocephalic damage to the brain tissue, although the rise in fluid pressure may have other detrimental effects.

6.2.3 Increased viscosity of CSF

An other potential cause of hydrocephalus reported clinically is an increase in the viscosity of the CSF, for instance due to haemorrhage in the ventricles. Since blood has a higher viscosity than CSF we might imagine that intraventricular bleeding would lead to a thickening of the fluid in the system and hence to an increase in pressure and a deformation in the brain. Should some protein enter the CSF system, perhaps as the result of an intraventricular infection or a malformation of the choroid plexus, the increase in viscosity would be likely to be even more pronounced. We have modelled this by varying the value of the viscosity from $\mu = 8.91 \times 10^{-4} \text{Ns/m}^2$, its physiological value, to $\mu = 8.91 \times 10^{-2} \text{Ns/m}^2$, two orders of magnitude greater.

The effect of such an increase on the intraventricular pressure and displacement is shown in figure 12. Both the pressure and deformation exhibit an apparently linear dependence on viscosity, but as in the previous case, the effect on the pressure is far greater. This is because in our model the main consequence of an increase in the viscosity is impairment of the absorption

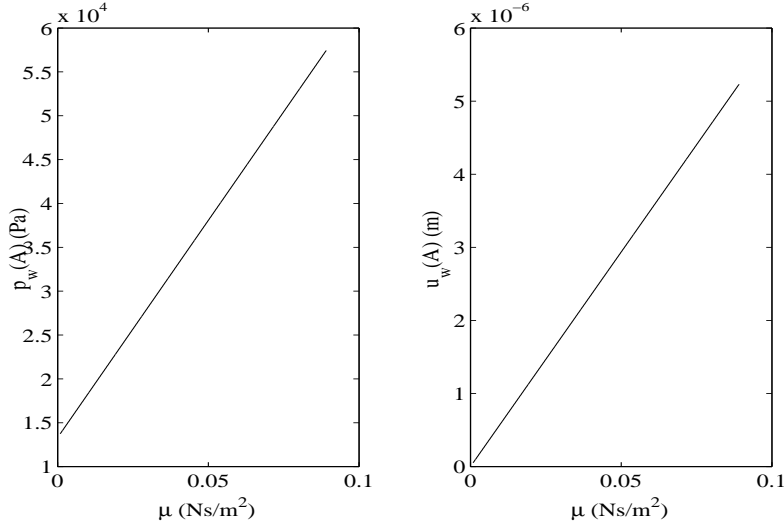


Figure 12: Effects of increasing the CSF viscosity, μ , on the ventricular pressure, $p_w(A)$, and wall displacement, $u_w(A)$

of fluid through the arachnoid villi, flow through the cerebral aqueduct is also impaired but the resistivity of this pathway is relatively low, so even a large increase in viscosity has little effect on the pressure gradient. Thus it seems that, based on our model, an increase in the viscosity of the CSF is unlikely to be a major cause of hydrocephalus. The only mention of hydrocephalus due to a change in fluid mechanical properties of the CSF in the medical literature refers to blood entering the ventricular system and a clot blocking the flow pathway, see Bradbury (1993). In terms of our model this would better correspond to the previous case of $d \rightarrow 0$ which, as we showed above, does lead to the symptoms of hydrocephalus, than to increased viscosity.

6.3 Treatments

Finally we model some of the treatments used in cases of hydrocephalus. The most effective, and hence the most widely used, treatment is shunting and so we shall consider it in some detail, but we begin with lumbar puncture.

6.3.1 Lumbar Puncture

In lumbar puncture some volume of CSF is removed from the patient, usually via the spinal cord, in order to relieve fluid pressure in the skull. In terms of our model we regard this as a step decrease in the intraventricular pressure, and hence in the displacement of the ventricle wall, without any permanent change in any of the material parameters. Clinically such a procedure has not proved to be successful in the long term, and is generally used only in severe cases where an immediate reduction of CSF pressure is required or in conjunction with another procedure such as shunting. The time dependent version of the model would appear to explain these observations; since all of the hydrocephalic steady states are stable (see Figure 5.8) any perturbation in $u_w(A)$ or $p_w(A)$ which is not accompanied by some change in the underlying material parameters will eventually decay, and $u_w(A)$ and $p_w(A)$ will eventually return to their

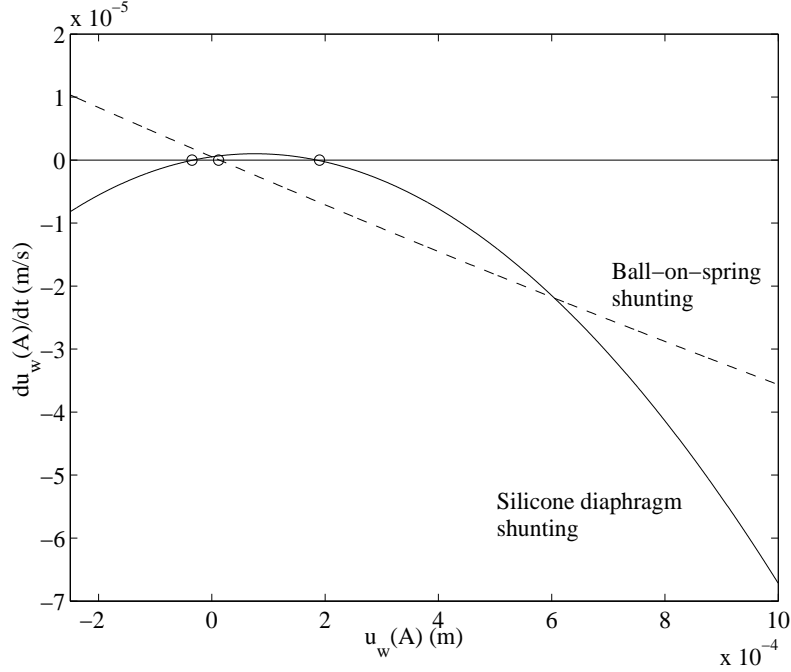


Figure 13: Phase plots of the ventricular wall displacement, $u_w(A)$ with shunting showing a single stable fixed point for ball on spring shunt (---) and two fixed points (one stable and one unstable) for silicone diaphragm shunt (—)

steady state pathological values. We do not include a plot of this behaviour since it would have a form the same as Figure 5.9, which shows the pressure and deformation moving to equilibrium.

6.3.2 Shunting

Shunt insertion is a major surgical procedure which entails implanting a tube with a valve leading from the ventricles into some point in the the body, normally an artery of the abdomen, where CSF is allowed to drain into the bloodstream. The intention of such a procedure is to create an alternative pathway for CSF drainage, and hence to relieve hydrocephalus. In addition to the difficulties normally associated with surgery on the brain there is the question of how much fluid to drain and how to control the rate of drainage, too much can lead to the collapse of the ventricles, so called ‘slit ventricle syndrome’, while too little will be insufficient to cure the illness. The main types of shunt currently used are ball-on-spring valves and silicone diaphragm valves which we model using equations (2.11) and (2.12) respectively. Note that in all cases in this section we consider the case of severe hydrocephalus where the aqueduct is blocked and $d = 0$.

Phase plots of the behaviour of the ventricle wall with shunt inserted are shown in figure 13, corresponding to a ball-on-spring shunt (linear pressure flow relationship) and to a silicone diaphragm shunt (quadratic pressure flow relationship). In each case there is a stable steady state close to $u_w(A) = 0$, indicating that shunting may be expected to be successful in reducing the deformation and returning the ventricles to their physiological size. Notice however that for a quadratic pressure flow relationship there is a second, unstable steady state at $u_w(A)$

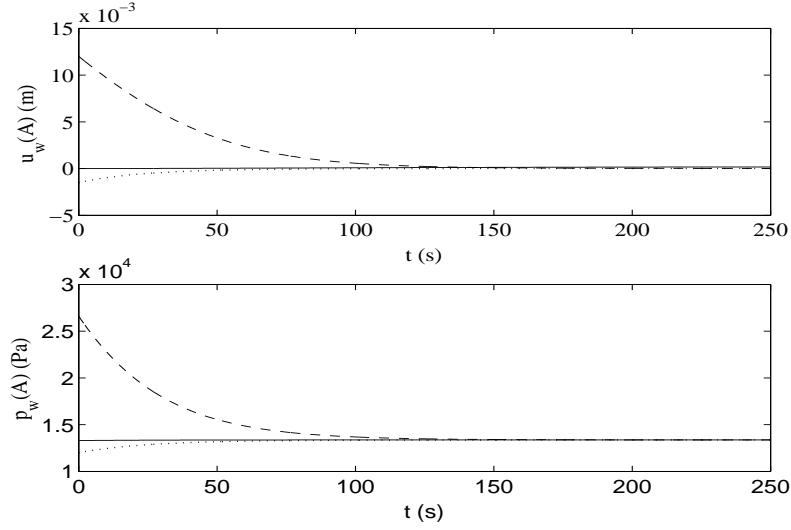


Figure 14: Time evolution of ventricular pressure, $p_w(A, t)$ and displacement, $u_w(A, t)$ following introduction of ball-on-spring shunt for three initial configurations, (---) severe hydrocephalus, (—) normal brain, (···) small negative perturbation

just less than zero. This indicates that should the radius of ventricles be perturbed below this second equilibrium point, by a blow to the head or the patient coughing say, the ventricular cavity will collapse, leading to slit ventricle syndrome. No such effect occurs with a linear pressure flow shunt, since there is only one, stable, steady state.

This contrasting behaviour is illustrated in figures 14 and 15, where we plot numerical solutions to equation (4.3) for the case of ball-on-spring and silicone diaphragm valves respectively. The figures show both the time evolution of the displacement of the ventricles and the intraventricular pressure for initial conditions of

$$\begin{aligned} u_w(A, 0) &= 1.2 \times 10^{-2} \text{m} && \text{(hydrocephalus),} \\ u_w(A, 0) &= 0 && \text{(normal),} \\ u_w(A, 0) &= -0.2 \times 10^{-2} \text{m} && \text{(negative perturbation).} \end{aligned}$$

In the case of a linear pressure-flow shunt, the brain returns to its healthy undeformed state for each initial condition. The time scale over which this occurs, 150 s, seems relatively short, though we do not have any clinical data with which to make a direct comparison. Our method of approximating the material parameter which describes the shunt resistance, S_1 , was fairly crude which may be the reason the model predicts such a short time for resolution of hydrocephalus. If the timescale for shunting to be effective is indeed rather longer than 150 s our results would explain why lumbar puncture is often used in conjunction with shunting in the treatment of hydrocephalus, the lumbar puncture quickly returns the ventricles to their undeformed configuration while the shunt prevents the intraventricular pressure from rising, hence maintaining the brain in its undeformed state.

The time evolution of the system with a silicone diaphragm shunt inserted is more complicated. For the first two initial conditions, corresponding to a hydrocephalic brain and a healthy brain, the behaviour of the deformation and the pressure is similar to the previous case, both return to a healthy state within a timescale of 100 s. In the case of a small negative

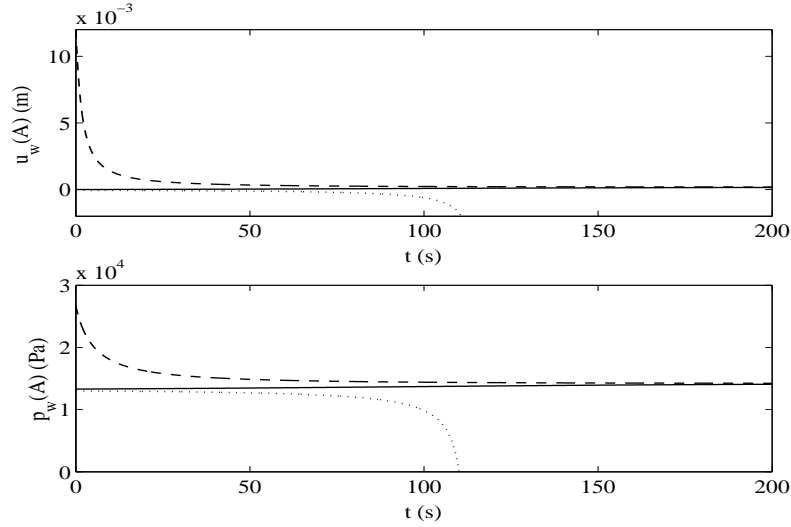


Figure 15: Time evolution of ventricular pressure, $p_w(A, t)$ and displacement, $u_w(A, t)$ following introduction of a silicone diaphragm shunt for three initial configurations, (---) severe hydrocephalus, (—) normal brain, (···) small negative perturbations silicone diaphragm shunting

perturbation to $u_w(A)$ the results are markedly different, both the radial displacement and intraventricular pressure fall farther below their normal values, until some kind of singularity appears at $t \approx 110$ s. At this point both drop very sharply and it is likely that a number of assumptions made in formulating the model, such as the small strain approximation, will cease to be valid. For this reason we do not attempt to model the behaviour of the system past this point, the crucial observation is that in the case of a valve exhibiting quadratic pressure volume relationship, shunting may introduce the possibility of collapse of the ventricular cavity.

7 Conclusions

The three main areas in which we have made significant refinements to existing models are: the specification of an anatomically realistic set of boundary conditions for the system, a review of the parameters to be used in describing the poroelastic properties of the brain tissue and a quasi-steady model for the time dependent behaviour of the system which gives the evolution of hydrocephalus or the evolution of clinical treatment.

An important step forward in modelling the anatomy of the brain comes with our inclusion of the cerebral aqueduct flow in addition to poroelastic flow through the parenchyma. This enables us to simulate the behaviour of the brain and CSF pathways in their normal, non-pathological state.

A two layered structure of the brain is useful since we can incorporate the differing material properties of the white and grey matter, though due to a lack of experimental data we are limited to prescribing different values for the permeability only. Our approach here is essentially the same as that of Kaczmarek et al. (1997), and the results for pressure and fluid content through the white and grey matter were similar to the findings of those authors.

The boundary conditions for the subarachnoid space are more sophisticated than in existing

models, where the authors have simply taken the fluid pressure to be fixed and the solid to either rigid (Nagashima et al. (1987), Kaczmarek et al. (1997) and Levine (1999)) or unconstrained Tenti et al. (1998). Our boundary conditions better enable us to consider the effects of a change in the resistivity of the arachnoid villi or the viscosity of the CSF and to model the deformation induced in the skull. For material parameters corresponding to an adult skull the resultant displacement is very small, so in some sense our boundary conditions are similar to those of a perfectly rigid outer layer of tissue. However, if values were known for the material properties of an infant's skull, our model could be used to analyse the magnitude of expected deformation due to congenital hydrocephalus and the effect of treatments such as compressive head wrapping.

We have considered the question of which values to use for the material parameters that appear in the governing equations. In particular we found what we believe to be suitable values for the Young's modulus and Poisson's ratio of the white and grey matter by reinterpreting the calculations made in Kaczmarek et al. (1997) using the concept of drained and undrained elastic constants in poroelasticity. We also computed values for the permeability of the white and grey matter and the Reynolds number for flow in the aqueduct.

The mathematical analysis of the development and treatment of hydrocephalus which we performed has not been attempted previously, we therefore believe that such an analysis represents a significant step towards a model of the illness which is both physically realistic and clinically useful. Our results for the onset of hydrocephalus due to stenosis of the aqueduct appear to be in agreement with clinical observations, both in terms of the stability of the hydrocephalic steady state and the time scale for its development. The results for some of the more unusual aetiologies, such as an increase in the viscosity of the CSF or impaired absorption in the subarachnoid space, were less successful in replicating clinical observations of hydrocephalus. This may however be due to our use of an inappropriate method of simulating of these aetiologies, rather than a weakness in our model overall.

Our results for the effect of shunting appear to be of some relevance, indicating that while shunting should in general be effective in reducing the intraventricular pressure which is the cause of hydrocephalus, certain types of shunt are likely to be more susceptible than others to over drainage of the ventricles. Since our model of shunting is somewhat crude it is the qualitative nature of these results, rather than the precise values for the location of the steady states which arise and the (short) timescale for the relief of the condition, which we believe to be of most interest. We also found that while lumbar puncture alone is ineffective in treating hydrocephalus, when combined with shunting it can quickly and permanently relieve the condition.

There are a number of extensions to this model which need to be considered. The very simple spherical geometry could be enhanced by using more sophisticated numerical solutions. Levine (1999) proposed a refinement to the governing equation for the fluid so that it includes the effect of trans-parenchymal absorption of CSF, that some fluid is absorbed by capillaries in the brain before it reaches the subarachnoid space. This leads to a new term in equations (3.2) and (3.3), which results in solutions in the form of hyperbolic sine and cosine functions. It may also be possible to incorporate the variable permeability model of Klachnar and Tarbell (1987) where again full numerical solutions would be necessary but as we have pointed out, such a vital extension requires better knowledge of the physical characteristics of the parenchyma. Since brain tissue is unlikely to display a linear stress-strain response, non-linear elastic theory, especially hyperelasticity, which has recently been applied with some success in other areas of

biomechanics (Humphrey, 2003), may be a way of formulating a more accurate constitutive relationship for the white and grey matter. Incorporating the porous nature of brain tissue into this type of non-linear theory is likely to present a mathematically challenging problem which, if resolved, may have a wide range of applications in biomechanics.

The linear and quadratic models used for ball-on-spring and silicone diaphragm shunts respectively are purely phenomenological in nature and the line fitting method of parameter estimation is likely to be approximate at best. This means that our results regarding the brain deformation and timescale for the effectiveness of shunting may need to be re-evaluated, but the qualitative nature of our findings should still be significant. We chose to use this approach since the only existing mathematical models of shunting in the literature (Buchheit et al. (1982) and Portnoy (1982)) are of an elementary form and we did not have sufficient time to construct a detailed model of our own. A pressure-flow relationship $S = S(\Delta p)$, based on a study of the hydrodynamic properties of shunts and validated experimentally, would therefore be of great use in the modelling of the treatment of hydrocephalus.

References

- Bickers D. and Adams R. (1949). *Hereditary Stenosis of the Aqueduct of Sylvius as a Cause of Congenital Hydrocephalus*. *Brain*, **72**:246–262.
- Biot M. (1941). *General Theory of Three Dimensional Consolidation*. *Journal of Applied Physics*, **12**:55–164.
- Bradbury M. (1993). *Anatomy and Physiology of CSF*. In Schurr P. and Polkey C., editors, *Hydrocephalus*.
- Buchheit F., Maitrot D., Healy J., and S. G. (1982). *How to choose the best valve*. In Choux M., editor, *Shunts and Problems in Shunts*.
- Czosnyka M., Czosnyka Z., Whithouse H., and Pickard J. (1997). *Hydrodynamic Properties of Hydrocephalus Shunts: UK Shunt Evaluation Laboratory*. *Journal of Neurology, Neurosurgery and Psychiatry*, **62**:43–50.
- Drake J., Kestle J., and Milner R. (1998). *Randomized Clinical Trials of Cerebrospinal Fluid Shunt Design in Pediatric Hydrocephalus*. *Neurosurgery*, **43**:294–305.
- Drake J. and Sainte-Rose C. (1995). *The Shunt Book*. Blackwell Science.
- Drossos A., Santomaa V., and Kuster N. (2000). *The Dependence of Electromagnetic Energy Absorption upon Human Head Tissue Composition in the range 300-3000 MHz*. *IEEE Transactions on Microwave Theory and Techniques*, **48**:1988–1995.
- Fay J. (1994). *Introduction to Fluid Mechanics*. MIT Press.
- Fung Y.C. (1993). *Biomechanics: Mechanical Properties of Living Tissues*. Springer-Verlag.
- Hakim S., Venegas J.G., and Burton J. (1976). *The Physics of the Cranial Cavity, Hydrocephalus, and Normal Pressure Hydrocephalus: Mechanical Interpretation and Mathematical Model*. *Surgical Neurology*, **5**:187–210.

- Holbourn A. (1943). *Mechanics of Head Injuries*. *The Lancet*, **2**:403–410.
- Humphrey J. (2003). *Continuum Biomechanics of Soft Biological Tissues*. *Proceeding of the Royal Society, London*, **A459**:3–46.
- Kaczmarek M., Subramaniam R., and Neff S. (1997). *The Hydromechanics of Hydrocephalus: Steady State Solution for Cylindrical Geometry*. *Bulletin of Mathematical Biology*, **59**:295–323.
- Klachnar M. and Tarbell J. (1987). *Modelling Water Flow through Arterial Tissue*. *Bulletin of Mathematical Biology*, **49**:651–669.
- Lakes R. (1993). *Materials with structural hierarchy*. *Nature*, **361**:511–515.
- Lakes R. (2002). *Making and characterizing negative Poisson’s ratio material*. *International Journal of Mechanics Engineering Education*, **30**:50–58.
- Levine D. (1999). *The Pathogenesis of Normal Pressure Hydrocephalus*. *Bulletin of Mathematical Biology*, **61**:875–916.
- Metz H., McElhaney J., and Ommaya A. (1970). *A Comparison of the Elasticity of Live, Dead and Fixed Brain Tissue*. *Journal of Biomechanics*, **3**:453–458.
- Miller K. and Chinzei K. (1997). *Constitutive Modelling of Brain Tissue: Experiment and Theory*. *Journal of Biomechanics*, **30**:115–1121.
- Nagashima T., Tamaki N., Matsumoto S., Horwitz B., and Seguchi Y. (1987). *Biomechanics of Hydrocephalus: A New Theoretical Model*. *Neurosurgery*, **21**:898–904.
- Portnoy H. (1982). *Hydrodynamics of shunts*. In Choux M., editor, *Shunts and Problems in Shunts*.
- Reulen H., Graham R., Spatz M., and Klatzo I. (1977). *Role of Pressure Gradients and Bulk Flow in the Dynamics of Vasogenic Brain Edema*. *Journal of Neurosurgery*, **46**:24–35.
- Sahay K. and Kothiyal K. (1984). *A Nonlinear Hyperelastic Model of the Pressure Volume Function of Cranial Components*. *International Journal of Neuroscience*, **23**:301–309.
- Sahay K., Mehrotra R., Sachdeva U., and Banerji A. (1992). *Elastomechanical Characterization of Brain Tissues*. *Journal of Biomechanics*, **25**:319–326.
- Sahay K.B. (1984). *On the choice of Strain Energy Function for Mechanical Characterisation of Soft Biological Tissues*. *Engineering in Medicine*, **13**:11–14.
- Sivaloganathan S., Drake J., and Tenti G. (1998). *Mathematical Pressure Volume Models of the Cerebrospinal Fluid*. *Applied Mathematics and Computation*, **94**:243–266.
- Smillie A. (2003). *A Biomechanical Model of the Pathogenesis and treatment of Hydrocephalus*. Master’s thesis, Oxford University.
- Stastna M., Tenti G., Sivaloganathan S., and J. D. (1998). *Brain Biomechanics: Consolidation Theory of Hydrocephalus. Variable Permeability and Transient Effects*. *Canadian Applied Mathematics Quarterly*, **7**:93–110.

- Tenti G., Drake J., and Sivaloganathan S. (2000). *Brain biomechanics: Mathematical Modelling of Hydrocephalus*. *Neurological Research*, **22**:19–24.
- Tenti G., Sivaloganathan S., and Drake J. (1998). *Brain Biomechanics: Steady-state Consolidation Theory of Hydrocephalus*. *Canadian Applied Mathematics Quarterly*, **7**:111–125.
- van Rietbergen H., Weinans B., Huiskes R., and Odgaard A. (1995). *A New Method to determine Bone Elastic Properties and Loading using Micromechanical Finite Element Models*. *Journal of Biomechanics*, **28**:69–81.
- Wang H. (2002). *Theory of Linear Poroelasticity: with Applications to Geomechanics and Hyrdogeology*. Princeton University Press.
- Weller R., Kida S., and Harding B. (1993). *Aetiology and Pathology of Hydrocephalus*. In Schurr P. and Polkey C., editors, *Hydrocephalus*.